Mechanical Alloying Synthesis of AB$_3$ Zirconium Substituted Intermetallic

Hassen Jaafar*, Chiheb Slama, Ines Sahli, Férid Mokhtar, Mohieddine Abdellaoui

Abstract: Several ternary RareEarth-Magnesium-Nickel intermetallics (RE-Mg-Ni) emerged in last decade for their specific hydrogen storage capability. Nickel is now considered among strategic metals with recurrent rising price, Magnesium although its good gravimetric facility suffers from frequent oxidation or irreversible poisoning. Zirconium alloys are recognized for their improved anti-corrosion properties with enhanced wear resistance for high temperature machinability in industrial applications or energy research purposes. We proposed in this paper double substitution possibility replacing Magnesium and reducing Nickel charge. We developed new generation of quaternary Zirconium-AB$_3$ intermetallic LaZr$_2$Ni$_5$Al$_4$ using mechanical alloying method. Two binary raw materials are involved in this alloying reaction, the first is LaNi$_5$ and the second is ZrAl$_2$ (Laves phase C14) and both precursors are achieved quasi-quantitively using high frequency induction melting. The final target AB$_3$ compound crystallizes in Trigonal system with space group R-3m (166) and following experimental conditions (Fritsch P7, Ω = 450 rpm) an acceptable synthesis yield (>80%) is obtained starting from 20 hours mechanical alloying. Rietveld refinement is performed to have real matrix parameters and AB$_3$ powder surface is analyzed using Scanning Electron Microscopy.

Keywords: intermetallic compounds; mechanical alloying; metals and alloys; Rietveld refinement; Zirconium

1 INTRODUCTION

Zirconium is known to have a very good resistance to corrosion and generally Zr-substitutions are elaborated on matrix-confined metallic structures regarding the wide range of physical properties that it can afford to the final material [1-3]. Several Zirconium based minerals are biocompatible (body implants) and furthermore Zircaloys can be used for high temperature applications (energy conversion) or ceramic materials due to their hard refractory properties (High Density Composites) giving excellent stability when exposed to aggressive chemicals [4-6].

In some cases, micro-indentation tests give or reach values up to 238 HV on Vickers hardness scale [7]. Energy storage reactions on Mg-RareEarth intermetallics can be easily found extensively in literature [8-10] but it is focused presently on synthesis methodology to develop novel quaternary AB$_3$ substituted intermetallic.

It was also demonstrated that various Zirconium hydrides formulae (ZrH, ZrH$_{1.6}$, ZrH$_2$, ZrH$_4$) can be formed following hydrogen reduction on Zirconium; and having good electrical conductivity or superconductivity characteristics [11]. Varying hydrogen amount makes ZrH$_x$ getting improved mechanical properties (regarding Zr-metallic element alone) and decreasing any crystal dislocations inside zirconium structure. So, the presence of hydrogen can serve as a controlling agent regarding the mechano-chemical properties of the end-up material [12].

Exploring new manufacturing techniques to enhance the microstructure and/or performance of Zirconium alloys (reducing the grain size for example to improve mechanical properties) constitute big challenge for their developments. Also, studying their behavior under extreme conditions is necessary to understand these new materials with improved stability and reliability.

We report in the present paper about a detailed synthesis and refinement processing of a new Zirconium based AB$_3$ compound LaZr$_2$Ni$_5$Al$_4$ using mechanical alloying method. This procedure involves the prefabrication of two binary precursors LaNi$_5$ and ZrAl$_2$ which are directly acquired using a high frequency induction melting.

2 MATERIALS AND METHODS

Elementary Lanthanum (La, ingot in oil, Merck Germany) and Nickel (Ni, Rod, Goodfellow USA) are used directly as purchased in atomic proportion 1:5 to carry out the binary precursor LaNi$_5$. For the Laves phase C14 precursor ZrAl$_2$, Zirconium (Zr, Rod, Goodfellow USA) and Aluminum (Al, Slag, Merck Germany) are also directly used from the provider in atomic proportion 1:2. All experiments with high frequency induction melting (Generator 25 kW) are done in inert atmosphere using secondary vacuum pump ($10^{-4} – 10^{-5}$ mbars).

LaZr$_2$Ni$_5$Al$_4$ intermetallic alloy was elaborated within a mechanical alloying configuration of Fritsch P7: Ω = 450 rpm, ball to powder ratio 36:1, jar volume 45 cm^3, and 5 stainless steel balls $\varnothing$ = 12 mm with mass m = 7.16 g. X-ray diffraction patterns are analyzed using a Bruker Diffractometer working with Copper Cu K$_{alpha}$ irradiation. Qualitative and quantitative analysis are accomplished respectively using following software HighScore and FullProf (for Rietveld). Scanning Electron Microscopy was done by an instrument type FEI Quanta 200.

3 RESULTS AND DISCUSSION
3.1 Characterization of Binary Precursor ZrAl$_2$

Electron Probe Micro-Analysis (EPMA) was carried out at first on several different regions and an example of EPMA micrography of ZrAl$_2$ sample is shown in Figure 1: we observe an overall primary gray zones and other minor black spots. The results of this microprobe analysis are given in Figs. 2 and 3 where it is obviously demonstrated that the gray areas correspond to ZrAl$_{2.04(10)}$ compound and minor black points to ZrAl$_{3.2(1)}$.

ZrAl$_2$ sample was also correctly refined using Rietveld method (ICSD reference data #150527) [13] as given in the

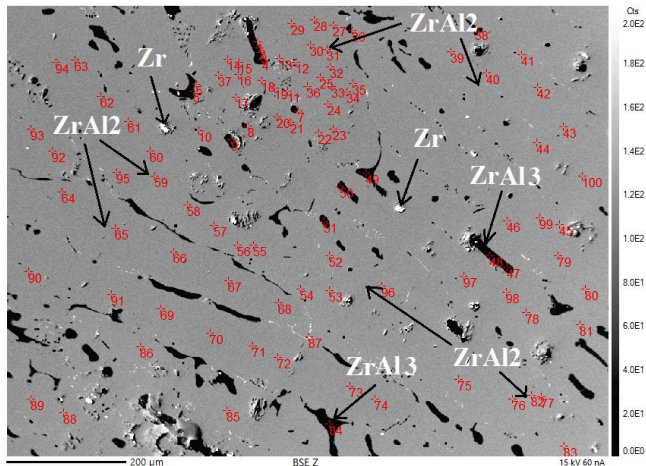following Fig. 4 and Tab. 1 estimating almost a quasi-quantitative yield for this synthesis.

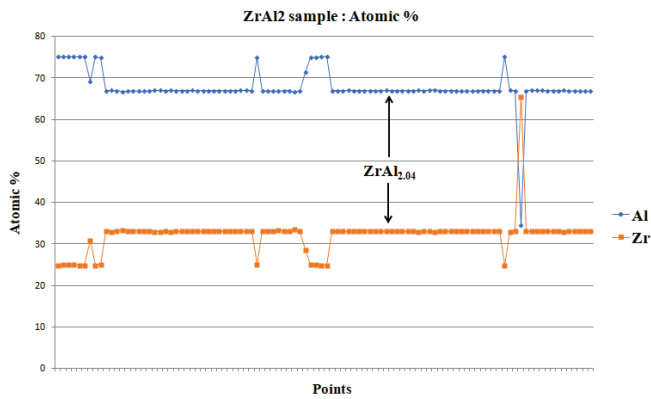

Figure 1 EPMA micrography of ZrAl₂ sample

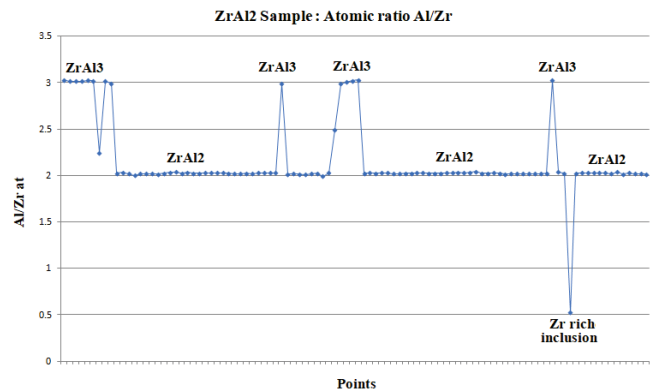**Figure 2** Atomic proportions obtained from EPMA analysis of ZrAl₂

Figure 3 Atomic ratios obtained from EPMA analysis of ZrAl₂

Table 1 Matrix parameters of refined sample ZrAl₂

Phase	Space group	Lattice parameters (Å)	V (Å³)	Weight fraction (%)	R_f	R_{Bragg}	χ^2
ZrAl₂	P6₃/mmc	$a = 5.27934$ (8) $c = 8.7428$ (2)	211.03	100	8.18	14.20	6.94

We have acceptable profile matching as verified from the values of conventional agreement factors (R_f, R_{Bragg}, χ^2), this

ZrAl₂ sample crystallizes in the space group P6₃/mmc (SG 194) with the following matrix parameters: $a = b = 5.27934$ (8) and $c = 8.7428$ (2).
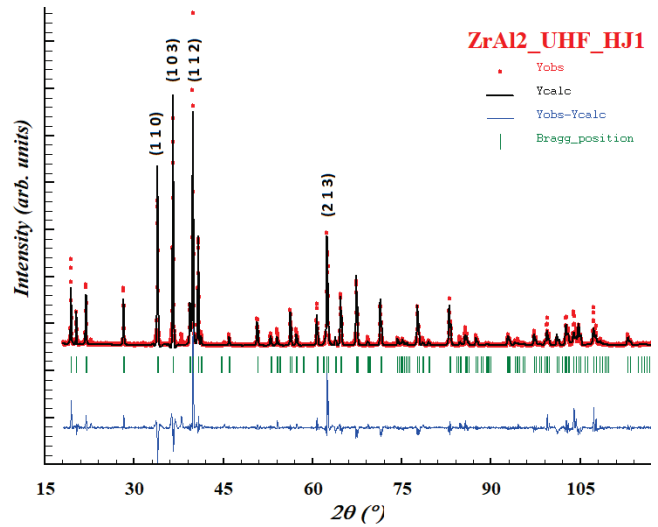

Figure 4 Example of Rietveld refinement for ZrAl₂ sample

3.2 Characterization of Binary Precursor LaNi₅

Many synthesis reaction pathways are existing in literature to easily achieve this intermetallic compound LaNi₅ [14]. We illustrate in the following Fig. 5 an insight on a micro-analysis mapping. Different focus points are selected, and the atomic proportion plot (Fig. 6) demonstrates that we obtain a precise nominal composition corresponding to LaNi₄.₉₇₍₅₎, obviously the atomic ratio calculation also given in Fig. 7 confirm that this sample appears to have practically uniform distribution of the desired phase.
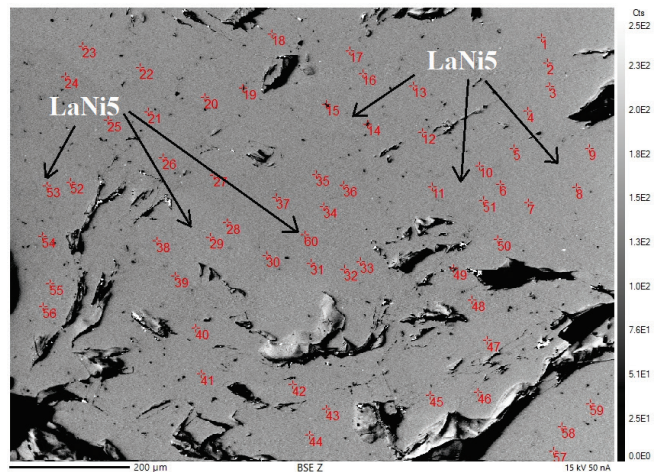

Figure 5 EPMA micrography of LaNi₅ sample

We have further undertaken the structural refinement to get the real matrix parameters using the same previous procedure with Rietveld method. This sample was refined according to the reference data (atomic positions and site occupations) from literature and patterns information from ICSD #155913 file assessment [15].
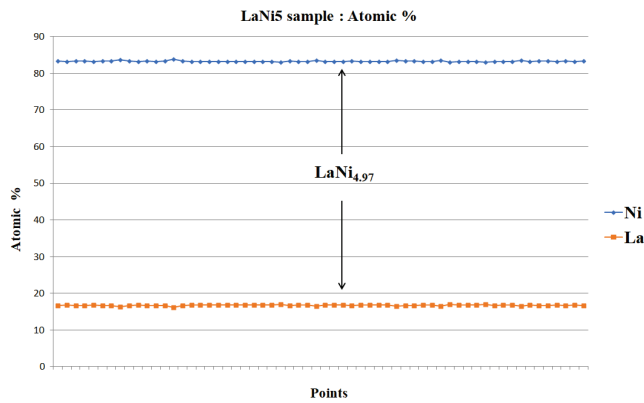
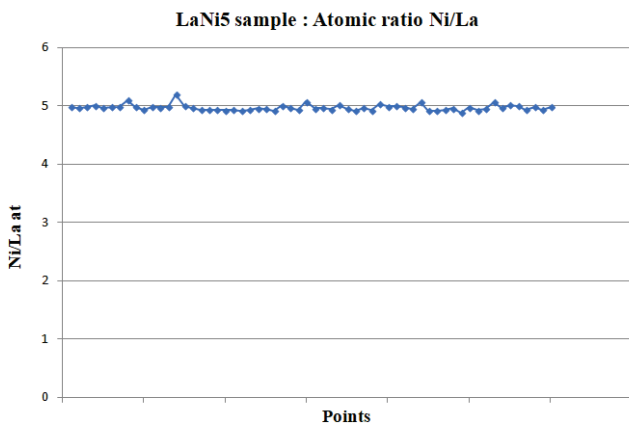**Figure 6** Atomic proportions obtained from EPMA analysis LaNi₅

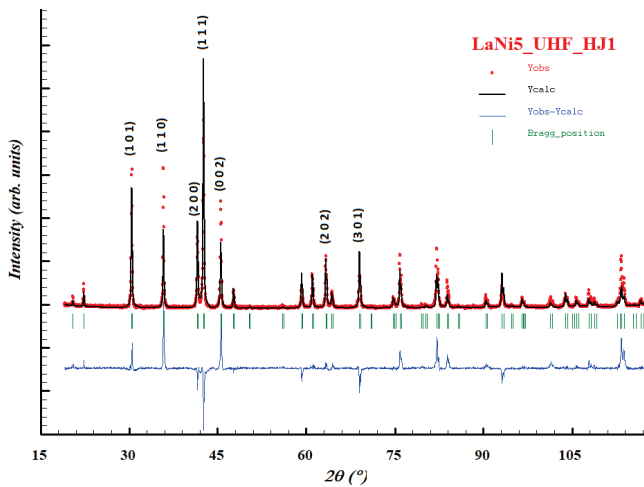**Figure 7** Atomic ratios obtained from EPMA analysis of LaNi₅

Figure 8 Example of Rietveld refinement for LaNi₅ sample

Table 2 Matrix parameters of refined sample LaNi₅

Phase	Space group	Lattice parameters (Å)	V (Å³)	Weight fraction (%)	R_f	R_{Bragg}	χ^2
LaNi₅	P6/mmm	$a = 5.0134$ (1) $c = 3.9831$ (1)	86.70	100	19.20	30.30	9.47

An example of structural refinement is simulated in the following Fig. 8 with (hkl) planes indexation. A very good
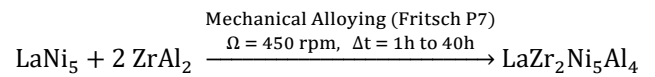
convergence is also mentioned regarding factors values in Tab. 2.

This Rietveld refinement confirm the homogenous phase stated and supporting previous atomic ratios evaluation by the microprobe analysis.

LaNi₅ is obtained within a quasi-total yield and the corresponding sample crystallizes in the space group P6/mmm (SG 191) with the following matrix cell parameters: $a = b = 5.0134$ (1) and $c = 3.9831$ (1).

3.3 Elaboration of AB₃ Alloy LaZr₂Ni₅Al₄

We have carried out in this section the intermetallic mechanical alloying reaction between the two precursors LaNi₅ and ZrAl₂ in molecular ratio 1:2 according to the following scheme:

$$\text{LaNi}_5 + 2\,\text{ZrAl}_2 \xrightarrow[\Omega = 450\ \text{rpm},\ \Delta t = 1\text{h to 40h}]{\text{Mechanical Alloying (Fritsch P7)}} \text{LaZr}_2\text{Ni}_5\text{Al}_4$$

The superposition of obtained diffractograms for all powder samples with different milling duration are represented in the stacking Fig. 9.
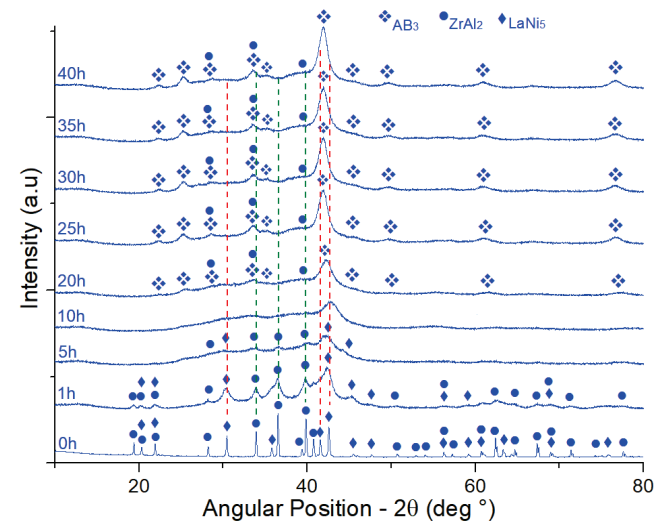

Figure 9 Stacking plot of alloyed samples with different duration

Powder evolution seems to be affected by clear amorphization starting from 1h processing where several initial diffraction peaks become overlapped within broadening signals, this observation is strongly accentuated up to 10h. Afterwards, different collected diffractions data are obviously displayed that certainly imply a new emerged intermetallic which will be further corroborated as major AB₃ compound following Rietveld refinement.

The minimum activation energy to achieve this new compound ($2\theta = 41.93°$) is accumulated in 20 h milling time (at disk rotation speed $\Omega = 450$ rpm, injected shock power 6.2 W/g) which corresponds to an overall kinetic energy of 124 Wh/g.

At first step and before AB₃ structural simulation, we tried to verify and testing the Rietveld processing on prior samples (duration 1 h and 5 h).

It is shown on consecutive Figs. 10 and 11 successful demonstration of Rietveld refinement applied on these alloyed samples where AB$_3$ target product is not yet appeared, allowed Bragg reflections are found to be attributed for initial AB$_5$ and AB$_2$ precursors (LaNi$_5$ and ZrAl$_2$).
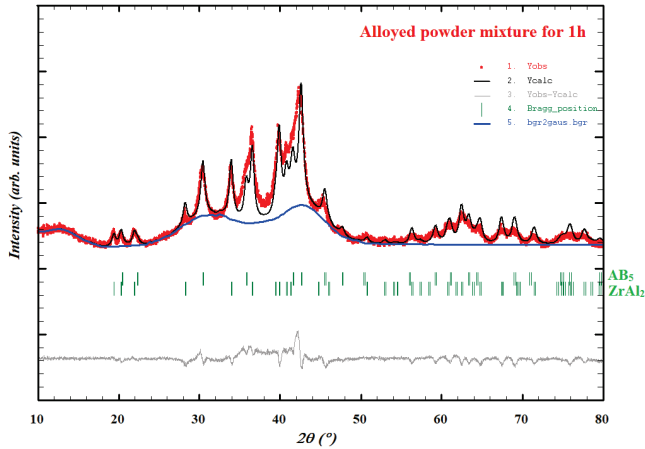

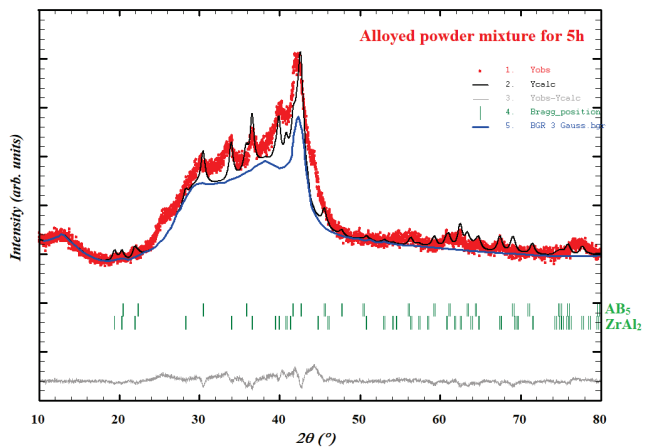**Figure 10** Rietveld refinement of alloyed powder mixture for 1 h

Figure 11 Rietveld refinement of alloyed powder mixture for 5 h

Table 3 Nearest-neighbor distribution of distances (partially crystalline intermetallics)

Position 2θ	Distance (Å)	FWHM	Attribution
Amorphous contribution in alloyed sample for 1 h duration			
34.32	2.61	8.95	AB$_2$
41.43	2.18	3.32	AB$_5$
Amorphous contribution in alloyed sample for 5 h duration			
29.74	3.01	5.45	N/A (intermediate)
36.48	2.46	8.37	AB$_2$
42.31	2.13	2.18	AB$_5$

We have found and perceive that computed amorphization contribution seems to be necessary and introduced in the program inputs to have subsequent appropriate convergence. In the first case of Fig. 10, the refinement was made possible unless two suitable amorphous related phases have been performed and deconvoluted using ABF Fit MacSoftware. The fitting can also evaluate as given in Tab. 3 the nearest-neighbor distribution of distances

corresponding to each amorphous contribution induced by mechanical alloying experiment.

It was further noted in second case of Fig. 11 that extra fitting contribution (2θ = 29.74°) was raised from ABF Fit simulation (Tab. 3) and might almost concern a transitional or intermediary state before reaching the desired crystalline compound. A very similar profiling shape was also observed at 10 h milling time, however refinement was limited regarding the very high broadening signals. According to Figure 9 and beginning from 20 h duration, the new compound appearing (at 2θ = 41.93°) seems to be stable even for long powder milling (up to 40h). Refinement was subsequently carried out (example Fig. 12) applying adequate crystal data (Tab. 4) conforming reference AB$_3$ material LaMg$_2$Ni$_9$ [16].

Table 4 Atomic positions and occupation factors in LaZr$_2$Ni$_5$Al$_4$

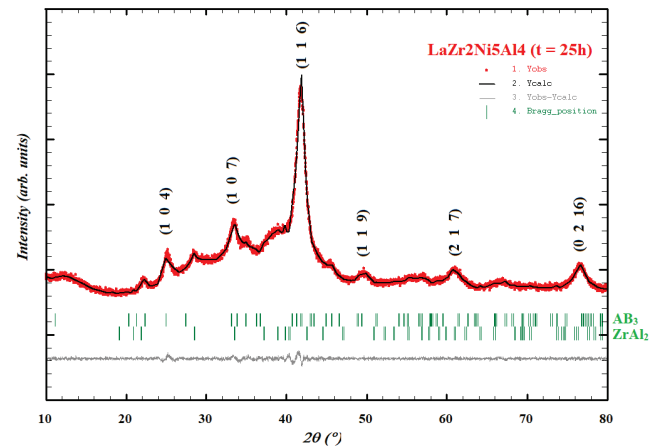| LaZr$_2$Ni$_5$Al$_4$ Cristal System: Trigonal / Space Group: R$\overline{3}$m (n° 166)					
	Wyckoff positions	x	y	z	Occ.
La	3a	0	0	0	1
Zr	6c	0	0	0.146(6)	1
Ni1	3b	0	0	1/2	0.555
Al1	3b	0	0	1/2	0.444
Ni2	6c	0	0	0.333(1)	0.555
Al2	6c	0	0	0.333(1)	0.444
Ni3	18h	0.5015(6)	0.4985(6)	0.0857(5)	0.555
Al3	18h	0.5015(6)	0.4985(6)	0.0857(5)	0.444

Figure 12 Rietveld refinement of alloyed powder mixture for 25 h

This new synthesized phase was refined in Rhombohedral R$\overline{3}$m space group, and successful Rietveld simulation was obtained in Fig. 12 showing the AB$_3$ inter-reticular planes index.

Alloying metallurgy demonstrates here that a double metal-substitution would be possible without altering the crystallographic system of reference structure LaMg$_2$Ni$_9$.

An overview of all convergent X-ray patterns refinements was summarized in this following tabulated datasheet (Tab. 5). It is therefore confirmed that major AB$_3$ phase (yield > 80%) formed for 20h operation (stay minor ZrAl$_2$) and without significant modification after 25 h.

Qualitative observations in X-ray stacking plot of Fig. 9 are corroborated regarding the quantitative results obtained from Rietveld refinements in Tab. 5. Very small amount of initial AB$_2$ precursor ZrAl$_2$ remain in powder, it is also

provided interestingly that we can reach almost 90 % of this intermetallic alloy with extended duration (40 h). But certainly, in scope of a potential industrial scale-up or commercialization outcome, the optimum and better energy/time ratio would be the samples corresponding to interval time between 20 - 25 h.

Table 5 Quantified phases found after mechanical alloying of different mixtures

Milling time	Phase	Space group	Lattice parameters (Å)	V (Å³)	Weight fraction (%)	R_f	χ^2
0 h	ZrAl₂	P 63/m m c	a = 5.27933(1) c = 8.74284(1)	211.03	42	26.4	12.8
	LaNi₅	P 6/m m m	a = 5.01338(1) c = 3.98306(1)	86.70	58	18.6	
1 h	ZrAl₂	P 63/m m c	a = 5.27933(1) c = 8.74284(1)	211.03	42	15.1	9.1
	LaNi₅	P 6/m m m	a = 5.01338(1) c = 3.98306(1)	86.70	58	14.8	
5 h	ZrAl₂	P 63/m m c	a = 5.27933(1) c = 8.74284(1)	211.03	42	29.8	6.8
	LaNi₅	P 6/m m m	a = 5.01338(1) c = 3.98306(1)	86.70	58	30.6	
20 h	AB₃	R-3m	a = 5.14787(1) c = 23.77881(1)	545.73	80	10.9	15.2
	ZrAl₂	P 63/m m c	a = 5.32196(1) c = 8.50014(1)	201.14	20	14.4	
25 h	AB₃	R-3m	a = 5.14313(1) c = 23.86803(1)	546.77	83	3.7	9.7
	ZrAl₂	P 63/m m c	a = 5.35148(1) c = 8.50242(1)	210.87	17	5.5	
30 h	AB₃	R-3m	a = 5.14207(1) c = 23.87111(1)	546.61	85	1.7	4.3
	ZrAl₂	P 63/m m c	a = 5.35182(1) c = 8.49647(1)	210.75	15	3.4	
35 h	AB₃	R-3m	a = 5.13574(1) c = 23.88005(1)	545.47	88	6.4	11.4
	ZrAl₂	P 63/m m c	a = 5.33861(1) c = 8.47411(1)	209.16	12	8.4	
40 h	AB₃	R-3m	a = 5.13565(1) c = 23.88844(1)	545.64	89	2.6	11.2
	ZrAl₂	P 63/m m c	a = 5.32945(1) c = 8.47399(1)	208.44	11	8.3	
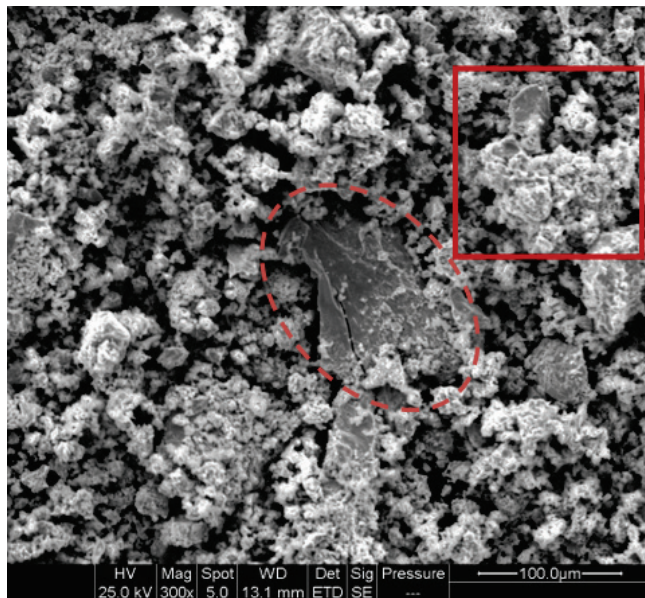
Figure 13 SEM morphology in secondary electron mode of sample AB₃ – 25 h

Intermetallic compound $LaZr_2Ni_5Al_4$ (25 h) crystallizes in the space group R-3m (SG 166) with the following matrix parameters: $a = b$ = 5.14313(1) and c = 23.86803(1). High precision given on crystal lattice indicate the appropriate convergence as well (see Tab. 5: R_f and χ^2) for the refinement simulations carried out in this section.

Table 6 Average atomic values obtained following Energy Dispersive Analysis of quaternary compound LaZr₂Ni₅Al₄

LaZr₂Ni₅Al₄-25h	Theoretical Atomic Percentages	Atomic Percentages found by EDX
%La	8.3	10.1
%Zr	16.7	15.9
%Ni	41.7	39.9
%Al	33.3	34.1

A sample of obtained mechanical alloyed powder at 25h was then analyzed using Scanning Electron Microscope SEM as given in next Fig. 13. In most concentrated focus SEM scan, surface morphology exhibited an overall homogeneous spherical-shape agglomerates (< 10 microns) and rare exceptions of localized bigger particles are observed corresponding to residual ZrAl₂ phase. It is also noted that Energy Dispersive Analysis (EDX) demonstrate according to Tab. 6 good convergence toward the nominal composition of intermetallic alloy developed $LaZr_2Ni_5Al_4$.

The average error found allover several spots (< 3 %) is considered very acceptable for this type of EDX analysis [17, 18]. Basically, the article is carried out to fulfill a detailed report on the technical assessment to achieve a new AB₃

intermetallic compound using a substitution transition element like Zirconium regarding its anti-corrosion advantages and extended high thermal operations as well energy conversion or storage. Melting point of Zirconium is about 1852 °C which constitute a big temperature gap (regarding low melting point for Aluminum and high oxidation sensitivity of Lanthanum) to overcome a quaternary intermetallic synthesis using high temperature melting furnace. The mechano-milling metallurgy processing presented in this case will be an efficient solution to elaborate withing an eco-compatible pathway the desired product.

4 CONCLUSIONS

In this study, we presented a novel mechanically alloyed Zr-AB$_3$ quaternary intermetallic. Metallurgy procedure involved two binary raw materials LaNi$_5$ and C14 Laves phase ZrAl$_2$, both of which are easily and completely produced by high frequency induction melting. X-ray diffraction data obtained for initial two compounds was validated by Rietveld refinement showing practically quasi-quantitative pattern in agreement with EPMA observations. Following mechano-milling procedure of binary precursors (Fritsch P7, $\Omega = 450$ rpm), more than 80 % of AB$_3$ crystalline phase LaZr$_2$Ni$_5$Al$_4$ was achieved after 20 hours duration which corresponds to equivalent activation energy of 124 Wh/g. Surface morphology demonstrated homogenous spherical particles less than 10 microns and Energy Dispersive analysis confirmed the nominal composition of the desired intermetallic material. Further perspective will consist in determining the exacts energy storage properties: solid-gas gravimetric hydrogen capacity, other thermodynamic parameters could be elucidated from isotherms of sorption behavior at different temperatures to retrieve the enthalpy and equilibrium pressure. Another more important substitutions will be exchanging totally rare earth metals using more sustainable elements keeping high level of expectation about favorable energy rendering.

5 REFERENCES

[1] Evstyukhin, A. I., Korobkov, I. I., & Osipov, V. V. (1970). Intermetallic Compounds of Zirconium and Their Influence on the Corrosion Properties of Zirconium Alloys. *Soviet Atomic Energy*, 28, 262-267. https://doi.org/10.1007/BF01403912

[2] Zumdick, M. F., Hoffmann, R.-D., & Pöttgen, R. (1999). The Intermetallic Zirconium Compounds ZrNiAl, ZrRhSn, and ZrPtGa - Structural Distortions and Metal-Metal Bonding in Fe$_2$P Related Compounds. *Zeitschrift für Naturforschung*, 54b, 54-53. https://doi.org/10.1515/znb-1999-0111

[3] Chandra, T., Wanderka, N., Reimers, W. et al. (2010). Microstructure and Mechanical Properties of Zr-Co-Ni Intermetallic Compound. *Materials Science Forum*, 638-642, 1379-1383. https://doi.org/10.4028/www.scientific.net/MSF.638-642.1379

[4] Chopra, D., Jayasree, A., Guo, T. et al. (2022). Advancing dental implants: Bioactive and therapeutic modifications of zirconia. *Bioactive Materials*, 13, 161-178. https://doi.org/10.1016/j.bioactmat.2021.10.010

[5] King, D. J. M., Knowles, A. J., Bowden, D. et al. (2022). High temperature zirconium alloys for fusion energy. *Journal of Nuclear Materials*, 559, 153431. https://doi.org/10.1016/j.jnucmat.2021.153431

[6] Fahrenholtz, W. G., Hilmas, G. E., Talmy I. G. et al. (2007). Refractory Diborides of Zirconium and Hafnium. *Journal of the American Ceramic Society, 90*(5), 1347-1364. https://doi.org/10.1111/j.1551-2916.2007.01583.x

[7] Fuloria, D., Goel, S., Jayaganthan, R. et al. (2015). Mechanical properties and microstructural evolution of ultrafine grained zircaloy 4 processed through multiaxial forging at cryogenic temperature. *Transactions of Nonferrous Metals Society of China, 25*(7), 2221-2229. https://doi.org/10.1016/S1003-6326(15)63835-3

[8] Zhang, H., Zheng, X., Tian, X. et al. (2017). New approaches for rare earth-magnesium based hydrogen storage alloys. *Progress in Natural Science: Materials International, 27*(1), 50-57. https://doi.org/10.1016/j.pnsc.2016.12.011

[9] Bu, W., Liu, Q., Peng, W. et al. (2022). Hydrogen storage kinetics and thermodynamics of Mg-based alloys by rare earth doping and Ni substitution. *Journal of Chemical Technology Biotechnology, 97*(5), 1180-1189. https://doi.org/10.1002/jctb.7002

[10] Yartys, V. A. & Lototskyy, M. V. (2022). Laves type intermetallic compounds as hydrogen storage materials: A review. *Journal of Alloys and Compounds*, 916, 165219. https://doi.org/10.1016/j.jallcom.2022.165219

[11] Abe, K. (2018). High-pressure properties of dense metallic zirconium hydrides studied by ab initio calculations. *Physical Review B*, 98, 134103. https://doi.org/10.1103/PhysRevB.98.134103

[12] Liu, S-M., Ishii, A., Mi, S-B. et al. (2022). Dislocation-Mediated Hydride Precipitation in Zirconium. *Small, 18*(9), 2105881. https://doi.org/10.1002/smll.202105881

[13] Wilson, C. G. (1959). The crystal structure of ZrAl$_2$. *Acta Crystallographica*, 12, 660-662. https://doi.org/10.1107/S0365110X59001943

[14] Liang, G., Huot, J., Schulz, R. (2001). Hydrogen storage properties of the mechanically alloyed LaNi5-based materials. *Journal of Alloys and Compounds, 320*(1), 133-139. https://doi.org/10.1016/S0925-8388(01)00929-X

[15] Zhi-jian, F., Bo, C., Guang-ai, S. et al. (2006). Investigation of Compounds LaNi$_5$D$_x$ (x=0, 0.3) by Means of Neutron Powder Diffraction. *Atomic Energy Science and Technology*, 1, 111-115.

[16] Kadir, K., Sakai, T., & Uehara, I. (1997). Synthesis and structure determination of a new series of hydrogen storage alloys; RMg$_2$Ni$_9$ (R=La, Ce, Pr, Nd, Sm and Gd) built from MgNi$_2$ Laves-type layers alternating with AB$_5$ Layers. *Journal of Alloys and Compounds, 257*(1-2), 115-121. https://doi.org/10.1016/S0925-8388(96)03132-5

[17] Carlton, R. A., Lyman, C. E., & Roberts, J. E. (2004). Accuracy and precision of quantitative energy-dispersive x-ray spectrometry in the environmental scanning electron microscope. *Scanning, 26*(4), 167-174. https://doi.org/10.1002/sca.4950260404

[18] Newbury, D. E. & Ritchie, N. M. (2013). Is scanning electron microscopy/energy dispersive X-ray spectrometry (SEM/EDS) quantitative. *Scanning, 35*(3), 141-168. https://doi.org/10.1002/sca.21041

Authors' contacts:

Hassen Jaafar, Assistant Professor
(Corresponding Author)
Institut National de Recherche et d'Analyse Physico-chimique,
BiotechPole Sidi Thabet, 2020 Ariana, Tunisia
hassen.jaafar@inrap.rnrt.tn

Chiheb Slama, Associate Professor
Ecole Supérieure d'Ingénieurs de Medjez El Bab,
Université de Jendouba, 9070, Tunisia
chihebslama@yahoo.fr

Ines Sahli, Post-doc
Institut National de Recherche et d'Analyse Physico-chimique,
BiotechPole Sidi Thabet, 2020 Ariana, Tunisia
sahli.ines86@yahoo.fr

Férid Mokhtar, Full Professor
Centre National de Recherches en Sciences des Matériaux,
Technopark Borj Cedria BP73, 8027, Tunisia
mokhtar.ferid@inrst.rnrt.tn

Mohieddine Abdellaoui, Full Professor
Institut National de Recherche et d'Analyse Physico-chimique,
BiotechPole Sidi Thabet, 2020 Ariana, Tunisia
mohieddine.abdellaoui@gmail.com